Human Cognition-Inspired Robotic Grasping

Marco Monforte, Fanny Ficuciello and Bruno Siciliano

Abstract The hand is one of the most complex and fascinating organs of the human body. We can powerfully squeeze objects, but we are also capable of manipulating them with great precision and dexterity. On the other hand, the arm, with its redundant joints, is in charge of reaching the object by determining the hand pose during preshaping. The complex motion and task execution of the upper-limb system may lead us to think that the control requires a very significant brain effort. As a matter of fact, neuroscience studies demonstrate that humans simplify planning and control using a combination of primitives, which the brain modulates to produce hand configurations and force patterns for the purpose of grasping and manipulating different objects. This concept can be transferred to robotic systems, allowing control within a space of lower dimension. The lower number of parameters characterizing the system allows for embodying the control in machine learning frameworks, reproducing a sort of human-like cognition.

1 Postural Synergies in Human Beings

With 27 bones, 18 joints and 39 intrinsic and extrinsic muscles with over 20 degrees of freedom [1–3], the hand is one of the most complex biomechanical parts of the human body. A traditional point of view is that the brain controls each joint and muscle to generate forces for grasping objects [4, 5]. To date, however, most studies have emphasized the opposite [6]. An early attempt to characterize hand postures during grasping has been made in [7], describing two main categories: *precision grasps* and *power grasps*. In the first category, one or more fingers are positioned,

M. Monforte (✉) · F. Ficuciello · B. Siciliano
DIETI, Università degli Studi di Napoli Federico II, Naples, Italy
e-mail: marco.monforte@iit.it; marco.monforte3@gmail.com

F. Ficuciello
e-mail: fanny.ficuciello@unina.it

B. Siciliano
e-mail: bruno.siciliano@unina.it

M. I. Aldinhas Ferreira et al. (eds.), *Cognitive Architectures*, Intelligent Systems, Control and Automation: Science and Engineering 94,
https://doi.org/10.1007/978-3-319-97550-4_6

usually in opposition to the thumb, to exert the necessary pressure to avoid the object falling from the hand [8]. In the second category, the palm is involved in the grasp to constrain the object. Later on, other authors [9–12] proposed further categorizations, based on the configuration of the fingers and on the part involved in the contact with the object. The key point of all of these works is that the fingers are used to generate forces, and it is assumed implicitly that the hand configuration is linked to this goal. If this is true, the posture should not change over time, but rather, there should be a discrete set of postures, each one corresponding to a grip.

This problem has been further investigated in [13], which introduces for the first time the concept of *Postural Hand Synergies* to study how the human brain controls the hand pre-grasping without considering haptic feedback. The results of these studies have revealed that the hand is controlled using a number of principal motions. A combination of those motions allows for continuously changing from a power to a precision grasp preshaping.

The Principal Component Analysis (PCA), performed on a number of hand configurations measured on different subjects, has shown that the first two components account for >80% of the variance among the dataset, implying a huge reduction from the 15 degrees of freedoms (DoFs) used to define a simplified kinematic model of the human hand. Higher-order PCs provide additional information about the hand posture, providing small adjustments to the fingers' position.

Another relevant work, developed in [14], has been conducted to study whether the grasp can be described by a lower number of postural synergies and whether there are similarities between synergies in grasping different objects. Five subjects have performed different types of reach-to-grasp movement on objects of different size and shape, while 21 joint positions have been recorded along the entire movement thanks to markers and a four-camera video system. The SVD analysis used in this work has proved that the first eigenposture explains most of the variance in the configurations and is comparable across the subjects. The second eigenposture contributes to the opening of the hand to its maximum during the reaching phase and to the thumb and finger flexion during the closing phase. Finally, higher order eigenpostures contribute by adding further information to the hand shape, in particular, about the flexion of the PIPs and DIPs joints.

All of these works suggest that the human brain does not control each finger or muscle independently but it applies some patterns learned during the evolution process through its cognitive capabilities, aiming at optimizing and simplifying the control of such complex biomechanical structures.

2 Postural Synergies in Robotics

The continuous technological improvement of recent decades is leading the robotics field to spread exponentially throughout in our society. Robots should be provided with improved reasoning capabilities and sensorimotor skills in order to interact deftly with their surrounding environment. Anthropomorphic robotic hands con-

tribute to this purpose, providing great dexterity and manipulation capabilities. Their high number of joints, however, might represent a complication for planning and control, especially during interaction with the environment.

Therefore, the use of postural synergies holds great potential, implying a substantial reduction of the dimension of the grasp synthesis problem. Their computation requires human hand motion mapping on the robotic hand.

2.1 Mapping Human Hand Motion to a Robotic Hand

Human hand motion mapping is a quite challenging problem due to the complexity and variety of hand kinematics. To obtain an accurate estimation of the human hand posture, a reliable kinematic hand model and very precise motion tracking instruments are required.

A model-based approach has been proposed in [15], using the fully actuated anthropomorphic DEXMART Hand [16]. The method is based on the detection of the positions of the fingertips of the human hand with respect to the palm through a Kinect RGBD camera. Due to the obvious differences in size and kinematics of the human hand [17], 5 different subjects have been involved in the acquisitions. Each of them had to perform the 36 grasps, with different types of grasp and objects of different shape and size.

To obtain the measures of the fingertips with respect to the palm frame, we first need to compute the homogeneous transformation between the camera frame and the palm frame. This goal has been achieved by measuring a set of five reference points on a rigid panel fixed to the back of the hand. Thus, first and foremost, each subject has worn this panel on the opisthenar and has assumed an open-hand posture. Ten points have been detected: the fingertips and five points suitably placed on the panel (Fig. 1a). Once the transformation T_i between the camera and the palm frame of the i-th subject has been found, each subject performs the 36 configurations.

To map the human grasps on the DEXMART Hand, a Closed-Loop Inverse Kinematics (CLIK) algorithm [18] has been used to retrieve the hand configuration, starting from the measured fingertip positions. In the CLIK algorithm, the DEXMART hand kinematics, properly scaled according to the dimensions of the human hand has

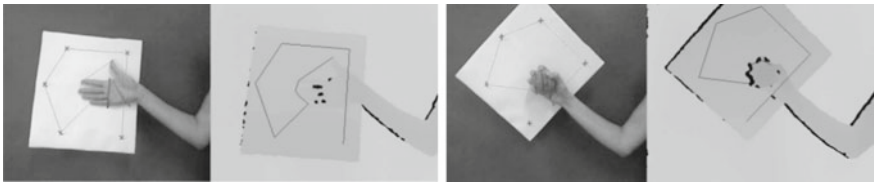

(a) Open-hand configuration. (b) Grasping an object.

Fig. 1 Snapshots from the fingertip position acquisition process

been used. The scaling of the robotic hand kinematics is obtained by multiplication of the D-H parameters for the ratio between the lengths of human and robotic fingers.

As a result, the matrix $\mathbf{C} \in \mathbb{R}^{36\times 15}$ has been created, where each $\mathbf{c}_i$ is a joint configuration representing the average of the five robotic hand configurations mapped from the five subjects.

2.1.1 Mapping to an Under-Actuated Robotic Hands

The same mapping method has been applied in [19] to an under-actuated robotic anthropomorphic hand to evaluate how the postural synergies change with respect to the fully-actuated case. The robotic hand considered in this work is the Schunk 5-Finger Hand (S5FH) [20]. Its structure is human-inspired, with dimensions comparable to those of humans and a weight of 1.3 kg. The hand possesses 20 degrees of freedom actuated by only 9 motors, thanks to mechanical synergies that regulate the kinematic couplings between the joints. These mechanical couplings are represented by the matrix S_m in (1), where the relationship between the 20 joints and the 9 motors is clear:

$$\underbrace{\begin{bmatrix} q_{t_o} \\ q_{t_{cm}} \\ q_{t_{mcp}} \\ q_{t_{dip}} \\ q_{i_s} \\ q_{i_{mcp}} \\ q_{i_{pip}} \\ q_{i_{dip}} \\ q_{m_{mcp}} \\ q_{m_{pip}} \\ q_{m_{dip}} \\ q_{p_o} \\ q_{r_s} \\ q_{r_{mcp}} \\ q_{r_{pip}} \\ q_{r_{dip}} \\ q_{l_s} \\ q_{l_{mcp}} \\ q_{l_{pip}} \\ q_{l_{dip}} \end{bmatrix}}_{\mathbf{q}} = \underbrace{\begin{pmatrix} 0.5 & 0 & 0 & 0 & 0 & 0 & 0 & 0 & 0 \\ 0 & 0.29 & 0 & 0 & 0 & 0 & 0 & 0 & 0 \\ 0 & 0.29 & 0 & 0 & 0 & 0 & 0 & 0 & 0 \\ 0 & 0.42 & 0 & 0 & 0 & 0 & 0 & 0 & 0 \\ 0 & 0 & 0 & 0 & 0 & 0 & 0 & 0 & 0.25 \\ 0 & 0 & 1 & 0 & 0 & 0 & 0 & 0 & 0 \\ 0 & 0 & 0 & 0.49 & 0 & 0 & 0 & 0 & 0 \\ 0 & 0 & 0 & 0.51 & 0 & 0 & 0 & 0 & 0 \\ 0 & 0 & 0 & 0 & 1 & 0 & 0 & 0 & 0 \\ 0 & 0 & 0 & 0 & 0 & 0.49 & 0 & 0 & 0 \\ 0 & 0 & 0 & 0 & 0 & 0.51 & 0 & 0 & 0 \\ 0.5 & 0 & 0 & 0 & 0 & 0 & 0 & 0 & 0 \\ 0 & 0 & 0 & 0 & 0 & 0 & 0 & 0 & 0.25 \\ 0 & 0 & 0 & 0 & 0 & 0 & 0.26 & 0 & 0 \\ 0 & 0 & 0 & 0 & 0 & 0 & 0.36 & 0 & 0 \\ 0 & 0 & 0 & 0 & 0 & 0 & 0.38 & 0 & 0 \\ 0 & 0 & 0 & 0 & 0 & 0 & 0 & 0 & 0.5 \\ 0 & 0 & 0 & 0 & 0 & 0 & 0 & 0.26 & 0 \\ 0 & 0 & 0 & 0 & 0 & 0 & 0 & 0.36 & 0 \\ 0 & 0 & 0 & 0 & 0 & 0 & 0 & 0.38 & 0 \end{pmatrix}}_{\mathbf{S}_m} \underbrace{\begin{bmatrix} m_0 \\ m_1 \\ m_2 \\ m_3 \\ m_4 \\ m_5 \\ m_6 \\ m_7 \\ m_8 \\ m_9 \end{bmatrix}}_{\mathbf{m}} + q_0, \qquad (1)$$

where $\mathbf{q}$ is the joints vector, $\mathbf{m}$ is the motors vector and $\mathbf{q}_0$ is an offset representing the vector of joint values when the motor positions are zero.

In this case, to map the subject fingertip positions for the 36 configurations to the robotic hand, the CLIK algorithm must take these couplings into account. The differential kinematics between the mechanical synergies subspace and the Cartesian space then becomes

$$\dot{\mathbf{x}} = \mathbf{J}_{h_s}\dot{\mathbf{m}}, \tag{2}$$

where $\mathbf{J}_{h_s}$ is the mechanical synergies Jacobian, computed as

$$\mathbf{J}_{h_s} = \mathbf{J}_h\mathbf{S}_m. \tag{3}$$

In (2), $\dot{\mathbf{x}}$ is the derivative of the five fingertips position vector $\mathbf{x} \in \mathbb{R}^{15}$ and $\mathbf{J}_h$ is the (15×20) S5FH Jacobian. The CLIK algorithm using the $\mathbf{J}_h^T$ has ultimately been used to map the grasps executed by the five subjects to the S5FH, leading, as with the DEXMART Hand, to the creation of a matrix of the configurations $\mathbf{C} \in \mathbb{R}^{36\times 9}$.

2.2 Hand Synergies Computation

Several methods have been proposed for computing the postural synergies. In [21–23], the synergies subspace is constituted by a matrix of constant eigengrasps, while in [24], the synergies are mapped directly to the robotic hand, resulting in a non-constant synergy matrix.

The first method has been used in [19] on the matrix $\mathbf{C} = \{\mathbf{c_1}, \ldots, \mathbf{c_{36}}\}$ after centering through the vector $\bar{\mathbf{c}}$, which is the mean configuration over the 36 grasps. In this way, the matrix $\mathbf{C}_{norm} = \{\mathbf{c}_1 - \bar{\mathbf{c}}, \ldots, \mathbf{c}_{36} - \bar{\mathbf{c}}\}$ of the grasp offsets with respect to $\bar{\mathbf{c}}$ has been computed. The Principal Component Analysis can now be applied by diagonalizing the covariance matrix of $\mathbf{C}_{norm}$ such that

$$\mathbf{C}_{norm}\mathbf{C}_{norm}^T = \mathbf{E}\mathbf{S}^2\mathbf{E}^T, \tag{4}$$

where the $(h \times h)$ orthogonal matrix $\mathbf{E}$ gives the directions of the variance of the data, while the diagonal matrix $\mathbf{S}^2$ represents the variance in each direction sorted by decreasing magnitude. Moreover, the matrix $\mathbf{E}$ represents the base matrix of the synergies subspace. Considering the entire (9×9) matrix, we obtain the whole configuration space of the hand, but, analyzing the variance described by the first j-th eigenvalues, it has been found that the first three principal components account for >85% of the variance, in accordance with what has been proved for the human hand in [13, 14]. This means that the matrix $\mathbf{C}$ can be reconstructed faithfully selecting the three predominant components from the PCA:

$$\hat{\mathbf{E}} = \left[\mathbf{e}_1\ \mathbf{e}_2\ \mathbf{e}_3\right], \tag{5}$$

while the configuration $\mathbf{c}_i$ can be projected onto the postural synergies subspace with a suitable choice of the parameter vector $\boldsymbol{\alpha} \in \mathbb{R}^3$ of the postural synergies:

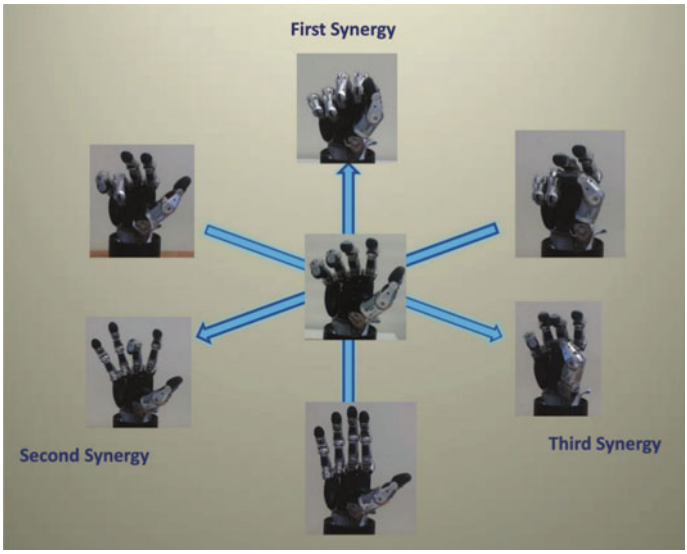

Fig. 2 Mean configuration and first three eigengrasps for the S5FH

$$\hat{\mathbf{c}}_i = \bar{\mathbf{c}} + \hat{\mathbf{E}} \begin{bmatrix} \boldsymbol{\alpha}_{1,i} \\ \boldsymbol{\alpha}_{2,i} \\ \boldsymbol{\alpha}_{3,i} \end{bmatrix}. \tag{6}$$

With these parameters, each synergy can be associated with a minimum and a maximum configuration, obtained by spanning the respective eigenvector through the minimum and maximum value of the associated weight $\boldsymbol{\alpha}_i$ without violating the joint limits. Figure 2 shows the mean configuration $\bar{\mathbf{c}}$ in the center and the minimum and maximum configuration from each synergy computed on the Schunk 5-Finger Hand.

It can be seen that the first synergy acts on the joints with a flexion movement, thus it is responsible for the opening and closing of the hand. The second synergy generates opposite motions for the metacarpophalangeal flexion and proximal interfalangeal flexion joints of the index and middle fingers (the ones without couplings). Finally, the third synergy acts mainly on the flexion and opposition of the thumb.

2.3 Grasping Control in the Synergies Subspace

Each grasp posture can be reconstructed from the linear combination of the restricted number of synergies adopted. From (6), it is easy to see that the coefficients of the synergies, characterizing the i-th configuration, can be obtained with a simple inversion:

Fig. 3 Two examples of reconstructed configuration

$$\begin{bmatrix} \boldsymbol{\alpha}_{1,i} \\ \boldsymbol{\alpha}_{2,i} \\ \boldsymbol{\alpha}_{3,i} \end{bmatrix} = \hat{\mathbf{E}}^{\dagger} \left(\mathbf{c}_i - \bar{\mathbf{c}} \right), \tag{7}$$

where $\hat{\mathbf{E}}^{\dagger}$ is the Moore-Penrose pseudo-inverse of $\hat{\mathbf{E}}$.

Of course, since the synergies provide only the final posture, the entire movement is not defined. However, we remember that in [14], it has been noticed that the human being opens its hand when reaching for an object to grasp it. Thus, it is licit to assume that a grasping movement might start from the initial configuration $\bar{\mathbf{c}}$, then go into an open-hand configuration $\mathbf{c}_0$, and finally towards the grasp configuration $\mathbf{c}_i$. In this way, the movement of the finger is obtained by means of a linear interpolation of the three coefficients $\boldsymbol{\alpha}$ corresponding to the three configurations mentioned above and computed with (7).

However, due to differences between human hand and robotic hand kinematics, some postures might not be accurate enough to allow for effective grasping of the object. This is also clear from Fig. 3, where we can see that not all the fingers are in contact with the objects. Thus, this simple approximation obtained by means of a few predominant synergies must be integrated with an appropriate control law, operating directly in the synergies subspace, in order to adjust the grasp and adapt the hand to the shape of the object. The approach proposed in [19] is a CLIK algorithm, in which a constant fingertip reference term is given by an approximation of the desired grasp in the synergies subspace. This term will determine a good hand pre-grasping. Afterwards, an additional term is designed to close the hand around the centroid of a virtual object, calculated as the mean position of the fingers employed in the grasp. The inverse kinematics is based on the synergies Jacobian given by $\dot{\mathbf{x}} = \mathbf{J}_{h_{ss}} \dot{\boldsymbol{\alpha}}$, with $\mathbf{J}_{h_{ss}} = \mathbf{J}_s \mathbf{S}_m \mathbf{S}_s$ and where $\mathbf{S}_s = \hat{\mathbf{E}}$ and $\boldsymbol{\alpha}$ are the synergies coefficients of the grasp posture. The latter are linked to the joint velocities by Eq. (8).

$$\dot{\mathbf{q}} = \mathbf{S}_m \dot{\mathbf{m}} = \mathbf{S}_m \mathbf{S}_s \dot{\boldsymbol{\alpha}}. \tag{8}$$

Fig. 4 Example of grasp configurations without (*left*) and with (*right*) the additional term based on the virtual object centroid

Moreover, to limit the grasping forces, the target position of the CLIK is limited through the measured motor current and by means of a defined threshold related to the texture of the object. The experiments have proved that a wide variety of objects can be grasped with this control strategy in the synergies subspace. The algorithm is stable and effectively modifies the finger positions to close the hand on the object and regulate the contact forces (Fig. 4).

2.4 Mapping Human Arm Motion to a Robotic Arm

The same concept of hand synergies can be extended to the human arm. A mo-cap suit has been used in [25]. The goal is the creation of a dataset of reaching-to-grasp movements (thus waveforms and no longer static postures) for a robotic arm for the computation of the arm synergies. The robotic arm is a KUKA Lightweight Robot 4+ [26], while the mo-cap system in question is the Xsens-MVN tool [27], composed by the Xsens suit and the proprietary software Moven Studio. The Xsens is a full body suit equipped with IMU sensors, named MTx, with advanced sensor fusion algorithms and wireless communication. Seventeen MTx are mounted on the most important parts of the human body, such as the head, chest, arm, forearm, hand, and so on. These MTx send their data to the MVN software, which, after an earlier calibration process, allows for real-time visualization of the human motion, playback and editing of the received data. An important option of this software is given by the possibility of sending data to third applications. Using an UDP/TCP-IP socket, the MTx data have been sent to the robotic arm using a mapping method that exploits the fact that the KUKA LWR presents 7 degrees of freedom, like the human arm. This has enabled a faithful replication of the master's movements.

To map her/his arm motion to the KUKA LWR 4+, the human master has to wear the Xsens suit (Fig. 5). After the calibration procedure provided by the software, the unit quaternions of the arm, forearm and hand, $\mathcal{Q}_{arm}$, $\mathcal{Q}_{forearm}$ and $\mathcal{Q}_{hand}$, are continuously received from the C++ script, which is charged with controlling the robotic arm by means of two CLIK algorithms. The first CLIK receives $\mathcal{Q}_{arm}$ and solves for the first three joints of the KUKA. The second CLIK receives $\mathcal{Q}_{hand}$ and solves for the other four joints of the robot arm. The elbow is a redundant joint

Fig. 5 The human master wearing the Xsens suit in order to telemanipulate the KUKA LWR 4+ and S5FH hand-arm system

controlled in the null space of the robot Jacobian to impose the same angle between the human arm and forearm, computed from $\mathcal{Q}_{arm}$ and $\mathcal{Q}_{forearm}$ with (9):

$$\theta_{elbow} = \arccos\left(\frac{\mathbf{v}_a \mathbf{v}_f}{\|\mathbf{v}_a\|\|\mathbf{v}_f\|}\right), \tag{9}$$

where $\mathbf{v}_a$ and $\mathbf{v}_f$ are the respective directions of the arm and the forearm.

Using this setup, 38 grasps of balls and cylinders, of different shapes and sizes, and with precision and power configurations have been performed. Since each acquired motion has a different duration, a data conditioning process has been carried out using Dynamic Time Warping (DTW) [28], in order that all of the same time length t_f for the N samples may be reached. As a result, the matrix $\mathbf{M} \in \mathbb{R}^{38\times7\times N}$ of grasping movements has been obtained.

2.5 *Arm Synergies Computation*

The approach presented in Sect. 2.2 for computing the hand postural synergies uses the PCA technique on static configurations. To compute motion arm synergies, an extension for multivariate waveforms of the PCA, namely Multivariate Functional Principal Component Analysis (MFPCA), has been used. A well-recognized procedure for computing the MFPCA does not exist at the moment. A first approach has been proposed in [29] and consists in stacking the waveforms recorded for each demonstration and then performing a common Univariate Functional Principal Component Analysis. The computed FPCA are then divided by the number of variables, obtaining the single FPCs. Extensions of the clustering problem and of data analysis of different dimensional domains have been respectively proposed in [30] and [31].

These works have an approach based on the Karhunen-Loeve representation of the data. A different method is illustrated in [32], in which the MFPCA is computed by performing the PCA at each time step and then interpolating the results. Further details about the theory behind the Univariate FPCA and the Multivariate FPCA can be found in [31].

According to the Karhunen-Loeve theorem, each grasping movement

$$\mathbf{m}_i(t) = \left(m_i^{(1)}(t), m_i^{(2)}(t), \ldots, m_i^{(7)}(t)\right) \quad \text{with} \quad t \in \left[0, t_f\right], \quad i = 1, \ldots, 38 \tag{10}$$

can be seen as a realization of a stochastic process and, under some assumptions, can be decomposed as

$$\mathbf{m}_i(t) = \boldsymbol{\mu}(t) + \sum_{k=1}^{\infty} \xi_{ik} \boldsymbol{\varphi}_k(t) \quad \text{with} \quad t \in \left[0, t_f\right], \tag{11}$$

where $\boldsymbol{\mu}(t)$ is the vector of the mean functions of the joints, $\boldsymbol{\varphi}_k$ is the vector of the k-th FPCs and ξ_{ik} is the k-th coefficient (or *score*) of the respective FPC for the i-th demonstration (Fig. 6). Thus, by truncating the sum to K terms, it is possible to approximate and parametrize each grasping movement with K scalar coefficients.

In analogy with the postural synergies of the hand, the function $\boldsymbol{\varphi}_k$ represents the waveform of a synergy, while the coefficient ξ_{ik} modulates the latter to obtain the movement.

From the MFPCA application on the matrix $\mathbf{M}$, 7 mean functions $\left[\mu^{(1)}(t), \ldots, \mu^{(7)}(t)\right]$ of the KUKA joints are obtained, K eigenfunctions $\left[\varphi_1^{(j)}(t), \ldots, \varphi_K^{(j)}(t)\right]$ for each joint j representing the basis of the subspace for each

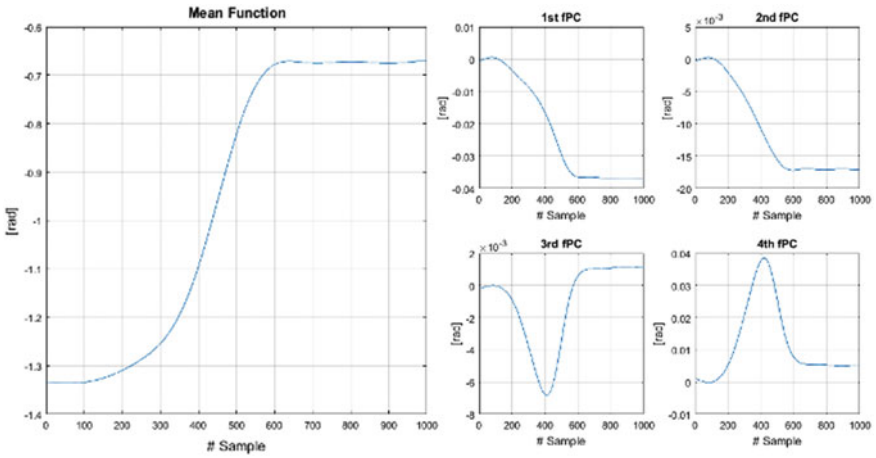

Fig. 6 Example of a mean function and the first 4 FPCs computed for the 5th joint

joint, and a matrix $\boldsymbol{\Xi} \in \mathbb{R}^{38\times K}$, where each row contains the scores of the respective demonstration.

From the analysis of the eigenvalues, it has been found that $K = 2$ FPCs are enough to cover >90% of the variance.

3 Combining Synergies with Machine Learning

From Sects. 2.2 and 2.3, it is clear that synergic patterns can be computed to reduce the number of parameters so as to control a high DoFs device.

In order to generalize the grasping strategy, a supervised learning system can be trained with the goal of learning the non-linear function that links the object's characteristics to its coefficients, so as to estimate the synergies coefficients for new objects. By selecting appropriate input features, such as the object type, its dimensions and/or the type of grasp, a database of configurations can be created, as in [19]. Applying the synergies computation to this database, a training set can be obtained associating the synergies coefficients with each example (thus, with each grasp performed). In this way, a Neural Network model can be trained with one of the several existing methods. Close attention, of course, must be paid to the creation of the training set, which has to cover a large variety of object shapes and sizes, and to the model hyperparameters tuning, such as learning rate, regularization term (to prevent underfitting and overfitting), number of hidden layers and number of hidden units. Anyway, a small percentage of error is always present when using neural networks. In the case of synergies, this is due first and foremost to the approximation introduced by their computation, and then to other reasons, like the training procedure itself.

To compensate for this error, in [33], a Reinforcement Learning strategy has been integrated directly into the synergies subspace. In particular, a modified version of the Policy Improvement with Path Integrals (PI^2) algorithm [34, 35] has been used. The policy update uses a probability-weighted averaging, without the needs of a gradient estimate and avoiding numerical instabilities due to matrix inversions. The synergies coefficients obtained from the neural network initialize the vector $\boldsymbol{\theta}$, representing the mean value of a Multivariate Gaussian distribution. From the latter, a number K samples are executed. K is defined by the user, along with the number of iterations of the algorithm, the initial covariance matrix $\boldsymbol{\Sigma}_{init}$ of the Multivariate Gaussian and a decay rate of $0 < \gamma \leq 1$. The PI^2 extracts these K samples and evaluates them, using a function based on the grasp quality index defined in [36] and already used in [19]. After the evaluation, the mean of the Multivariate Gaussian is updated by weighting the previous trials and moving $\boldsymbol{\theta}$ toward those attempts with better reward. The covariance matrix, instead, is multiplied by the decay rate, in order to reduce the dispersion of the subsequent trials from the good values obtained previously. The algorithm proceeds in this way until it reaches an optimal mean value for the Gaussian, with a covariance so small that the samples are too close to the mean to bring substantial differences.

The experiments are made with the robotic hand-arm system constituted by the KUKA LWR 4+ and the SCHUNK 5FH. Exploiting the hand and arm synergies computed in [19] and [25], two neural networks have been trained (one for the hand and one for the arm) using the Matlab NN Toolbox to provide the initial synergies parameters for a PI^2 algorithm. Human supervision has been necessary (but could be replaced in future by a vision system) to tell whether the object was grasped or not, in order to evaluate the reward function adopted (12)

$$r(\boldsymbol{\theta}_k) = V(\boldsymbol{\theta}_k) + \phi, \tag{12}$$

where $V(\boldsymbol{\theta}_k)$ is the measured quality index and ϕ is

$$\phi = \begin{cases} 0 & \text{if grasp succeeds} \\ 10^3 & \text{if grasp fails} \end{cases}, \tag{13}$$

which is chosen in order to penalize failed trials, and thus lead the convergence of the PI^2 toward the successful grasp.

4 Conclusions

The experiments carried out proved that the usage of 3 hand synergies and 2 arm synergies in a machine learning system composed by neural networks and reinforcement learning allows the robot to improve its grasping capabilities through a trial-and-error approach (Fig. 7). Machine learning techniques can be efficiently combined with synergies in order to create frameworks capable of reducing the complexity of control by taking inspiration from human cognitive architectures.

(a) Precision grasp of a ball.

(b) Power grasp of a cylinder.

Fig. 7 Improvement of the grasp during execution of the algorithm

Acknowledgements This research has been partially funded by the EC Seventh Framework Programme (FP7) within RoDyMan project 320992 and by the national grant MUSHA under Programma STAR linea 1.

References

1. Kapandji, I. A. (1970). *The physiology of the joints. Upper limb* (Vol. 1, 2nd ed., pp. 146–202). London: E. and S. Livingstone.
2. Tubiana, R. (1981). Architecture and function of the hand. In R. Tubiana (Ed.), *The Hand* (Vol. 1, pp. 19–93). Philadelphia, PA: Saunders.
3. Soechting, J. F., & Flanders, M. (1997). Flexibility and repeatability of finger movements during typing: Analysis of multiple degrees of freedom. *Journal of Computing Neuroscience*, *4*, 29–46.
4. Lemon, R. N. (1999). Neural control of dexterity: What has been achieved? *Experimental Brain Research*, *128*, 6–12.
5. Schieber, M. (1990). How might the motor cortex individuate movements? *Trends Neuroscience*, *13*, 440–445.
6. Schieber, M. (1995). Muscular production of individuated finger movements: The roles of extrinsic finger muscles. *Journal of Neuroscience*, *15*, 284–297.
7. Napier, J. R. (1956). The prehensile movements of the human hand. *Journal Bone and Joint Surgery*, 38B, 902–913.
8. Johannson, R. S., & Cole, K. J. (1992). Sensory-motor coordination during grasping and manipulative actions. *Current Opinion in Neurology*, *2*, 815–823.
9. Kamakura N., Matsuo M., Ishii H., Mitsuboshi F., & Miura Y. Patterns of static prehension in normal hands. *The American Journal of Occupational Therapy, 7*, 437–445.
10. Elliot, J. M., & Connolly, K. J. A. (1984). Classification of manipulative hand movements. *Developmental Medicine & Child Neurology, 26*, 283–296.
11. Klatzky, R. L., Pellegrino, J., McCloskey, B., Doherty, S., & Smith, T. (1987). Knowledge about hand shaping and knowledge about objects. *Journal of Motor Behavior*, *19*, 187–213.
12. Cutkosky, M. R., & Howe, R. D. (1990). Human grasp choice and robotic grasp analysis. In S. T. Venkataraman & T. Iberall (Eds.), *Dextrous robot hands* (pp. 5–31). New York: Springer.
13. Santello, M., Flanders, M., & Soechting, J. F. (1998). Postural hand synergies for tool use. *The Journal of Neuroscience*, *18*, 10105–10115.
14. Mason, C. R., Gomez, J. E., & Ebner, T. J. (2001). Hand synergies during reach-to-grasp. *Journal of Neurophysiology*, *86*, 2896–2910.
15. Ficuciello F., Palli G., Melchiorri C., & Siciliano B. (2013). A model-based strategy for mapping human grasps to robotic hands using synergies. In *Proceedings 2013 IEEE/ASME International Conference on Advanced Intelligent Mechatronics*.
16. Palli, G., Melchiorri, C., Vassura, G., Berselli, G., Pirozzi, S., Natale, C., De Maria, G., & May, C. (2012). Innovative technologies for the next generation of robotic hands. In B. Siciliano (Ed.), *Advanced Bimanual Manipulation*. Springer Tracts in Advanced Robotics (Vol. 80, pp. 173–218). Springer.
17. Grebenstein, M., Chalon, M., Hirzinger, G., & Siegwart, R. (2010). A method for hand kinematics designers 7 billion perfect hands. In *Proceedings 1st International Conference on Applied Bionics and Biomechanics* (pp. 357–362). Venice, Italy.
18. Siciliano, B., & Khatib, O. (Eds.). (2008). *Springer Handbook of Robotics* (2nd ed.). Springer.
19. Ficuciello, F., Federico, A., Lippiello, V., & Siciliano, B. (2017). Synergies evaluation of the SCHUNK S5FH for grasping control. *Springer Proceedings in Advanced Robotics*, *4*, 225–233.
20. Schunk hand webpage. http://www.schunk-modular-robotics.com/en/home/products/servo-electric-5-finger-gripping-hand-svh.html.

21. Ficuciello, F., Palli, G., Melchiorri, C., Siciliano, B. (2011). Experimental evaluation of postural synergies during reach to grasp with the UB Hand IV. In *Proceedings IEEE/RSJ International Conference on Intelligent Robots and Systems* (pp. 1775–1780). San Francisco.
22. Geng, T., Lee, M., & Hulse, M. (2011). Transferring human grasping synergies to a robot. *Mechatronics*, *21*(1), 272–284.
23. Sun, S., Rosales, C., & Suarez, R. (2010). Study of coordinated motions of the human hand for robotic applications. In *Proceedings IEEE International Conference on Robotics and Automation* (pp. 776–781). Anchorage, Alaska.
24. Gioioso, G., Salvietti, G., Malvezzi, M., & Prattichizzo, P. (2011). Mapping synergies from human to robotic hands with dissimilar kinematics: An object based approach. In *IEEE International Conference on Robotics and Automation, Workshop on Manipulation Under Uncertainty*. Shangai.
25. Ficuciello, F., Zaccara, D., & Siciliano, B. (2016). Learning grasps in a synergy-based framework. In *Springer Proceedings in Advanced Robotics* (Vol. 1, pp. 125–135). Cham.
26. KUKA Lightweight Robot 4+ webpage. https://www.kukakore.com/wp-content/uploads/2012/07/KUKA_LBR4plus_ENLISCH.pdf.
27. Xsens-MVN webpage. https://www.xsens.com/products/xsens-mvn.
28. Giorgino, T. (2009). Computing and visualizing dynamic time warping alignments in R: The dtw package. *Journal of statistical Software*, *31*(7), 1–24.
29. Ramsay, J. O., & Silverman, B. W. (2005). *Functional Data Analysis*. Springer.
30. Jacques, J., & Preda, C. (2004). Model-based clustering for multivariate functional data. *Computational Statistics & Data Analysis*, *71*, 92–106.
31. Happ, C. (2015). Multivariate functional principal component analysis for data observed on different (dimensional) domains. *Journal of the American Statistical Association*.
32. Berrendero, J., Justel, A., & Svarc, M. (2011). Principal components for multivariate functional data. *Computational Statistics & Data Analysis*, *55*(9), 2619–2634.
33. Ficuciello, F., Zaccara, D., & Siciliano, B. (2016). Synergy-based policy improvement with path integrals for anthropomorphic hands. In *Proceedings IEEE/RSJ International Conference on Intelligent Robots and Systems* (IROS2016) (pp. 1940–1945).
34. Theodorou, E., Buchli, J., & Schaal, S. (2010). A generalized path integral control approach to reinforcement learning. *Journal of Machine Learning Research*.
35. Stulp, F., & Sigaud, O. (2012). Path integral policy improvement with covariance matrix adaptation. In *Proceedings of the 29 International Conference on Machine Learning*.
36. Bicchi, A. (1994). On the closure properties of robotic grasping. *International Journal of Robotics Research*, *14*(4), 319–334.